Available online at www.sciencedirect.com
SCIENCE DIRECT®
Chemical Physics 325 (2006) 138–151
Chemical Physics
www.elsevier.com/locate/chemphys

Structural and vibrational characterization of the organic semiconductor tetracene as a function of pressure and temperature

Adam M. Pivovar [a,*], Joseph E. Curtis [a,*], Juscelino B. Leao [a], Reid J. Chesterfield [b], C. Daniel Frisbie [b,*]

[a] NIST Center for Neutron Research, National Institute of Standards and Technology, 100 Bureau Drive Stop 8562, Gaithersburg, MD 20899-8562, USA
[b] Department of Chemical Engineering and Materials Science, University of Minnesota, Minneapolis, MN 55455-0132, USA

Received 30 June 2005; accepted 3 January 2006
Available online 24 March 2006

Abstract

Neutron powder diffraction and inelastic neutron scattering measurements were performed on crystalline tetracene, a molecular semiconductor of triclinic crystal structure that adopts a herringbone layered motif, as a function of pressure up to 358 MPa. In combination with theoretical and simulated computations, these measurements permit detailed characterization of the structural and vibrational changes of tetracene as a function of pressure. Powder diffraction at 295 K reveals anisotropic modification of the crystal structure with increasing pressure. Particularly, the unit cell parameters associated with the two-dimensional herringbone layers of the solid state structure displayed continuous change at all measured pressures, whereas perpendicular to the herringbone layers the structure remains relatively unchanged. The measured compressibilities along the [1 0 0], [0 1 0], and [0 0 1] crystal axes are -3.8×10^{-4}, -1.9×10^{-4}, and -3.4×10^{-4} Å/MPa, respectively. Inelastic neutron scattering spectra were collected at several pressures in the 25–75 and 0–25 meV energy ranges using a filter analyzer and a Fermi chopper time-of-flight spectrometer, respectively. Assignment of the spectral peaks to specific intramolecular vibrational modes has been accomplished using ab initio density functional theory calculations and the low energy lattice phonon modes were interpreted from the results of molecular dynamics simulations at 1 atm and 358 MPa. Anisotropic behavior parallel to that observed in the structural measurements is also apparent in both the intramolecular and lattice phonon vibrational dynamics. Intramolecular vibrations having atomic displacements entirely within the plane of the molecule's aromatic ring remain unchanged with increasing pressure while vibrations with atomic displacements perpendicular to the molecular plane shift to higher energy. The lattice phonons display a similar anisotropy with increasing pressure. Phonon modes propagated within the herringbone layer are significantly shifted to higher energy with increasing pressure relative to the modes with displacements primarily perpendicular to the layers. Overall, both the planar internal geometry and the layered arrangement of the tetracene molecules significantly influence the observed structural and vibrational behavior with increasing pressure.

Keywords: Neutron scattering; Structure; Dynamics; Vibrations; Phonons; Ab initio calculations; Molecular dynamics; Organic semiconductors; Tetracene; Transport; Conduction

1. Introduction

Organic semiconductors are promising materials for optoelectronic applications. Crystals and polycrystalline films based on phenylene, thiophene, and fused ring acene molecular units have been utilized in the construction of

* Corresponding authors. Tel.: +1 301 975 8396.
E-mail addresses: adam.pivovar@nist.gov (A.M. Pivovar), joseph.curtis@nist.gov (J.E. Curtis), frisbie@cems.umn.edu (C.D. Frisbie).

0301-0104/$ - see front matter © 2006 Elsevier B.V. All rights reserved.
doi:10.1016/j.chemphys.2006.01.041

functional devices such as light emitting diodes and field effect transistors [1–8]. In these materials, light emission and charge transport properties are attributable both to the internal molecular structure and the molecular packing in the crystalline solid state. Both the intramolecular and intermolecular electronic distributions affect the luminescence quantum yield and charge transport properties of these materials. A deeper understanding of the relationship between intramolecular and intermolecular interactions and the internal conformation, relative molecular orientation, vibrational behavior, and electronic distribution in molecular solids should promote advancement of functional organic devices.

One approach to tuning inter- and intramolecular interactions in organic semiconductors is to vary the applied hydrostatic pressure [9–15]. Increasing pressure decreases intermolecular distances in a crystal, creating increased electron orbital overlap between adjacent molecules [11]. Qualitatively, one predicts that carrier mobility will therefore increase with increasing hydrostatic pressure. *Quantitative* understanding of the pressure dependence of the mobility (which is a tensor quantity), however, depends on knowledge of the carrier transport mechanism and changes in the crystal structure and vibrational/phonon spectrum of the material with applied pressure. It has been found that very clean single crystals of oligoacenes (fused ring organic semiconductor materials) display an inverse power law dependence of the mobility on temperature, which is indicative of delocalized, band-like transport [16]. On the other hand, other mobility measurements are susceptible to interpretation of charge carrier transport through a hopping-like motion [17–21]. In principle, complementary pressure dependent transport measurements, coupled with theoretical calculations, would allow a more precise understanding of the role of intermolecular interactions on electronic bandwidth, carrier delocalization and effective mass, providing further insight into the transport mechanisms responsible for charge mobility in these materials.

Pressure dependent charge transport and photoconductivity have in fact been measured previously in several oligoacenes (e.g., anthracene, tetracene, pentacene). For example, several investigators have observed an increase of charge carrier mobility with increasing pressure in oligoacene crystals [20,22,23]. Photoconductivity experiments on tetracene (see Fig. 1) as a function of pressure have been performed by Rang et al. between ambient pressure and 600 MPa [10]. Their results indicated a linear increase in photocurrent up to ~300 MPa, with a drastic reduction in the photoconductive properties between 300 and 600 MPa. The decrease in photocurrent was attributed to a reported pressure induced phase transition at 300 MPa as determined by fluorescence resonance measurements in a magnetic field [24,25]. A recent Raman spectroscopy investigation, however, observed that the pressure induced phase transition of tetracene occurs at pressures much greater than 300 MPa and that a primary polymorph of tetracene may contain impurities of second polymorph at room temperature and ambient pressure [26].

To fully interpret the temperature and pressure dependence of charge transport in organic semiconductor crystals it is also necessary to determine the temperature and pressure dependence of the crystal lattice parameters and the vibrational behavior. In this paper, we examine the pressure dependent physical properties of tetracene by measuring changes to the structural parameters and the low energy vibrational dynamics up to 360 MPa. For these measurements, we have used neutron powder diffraction

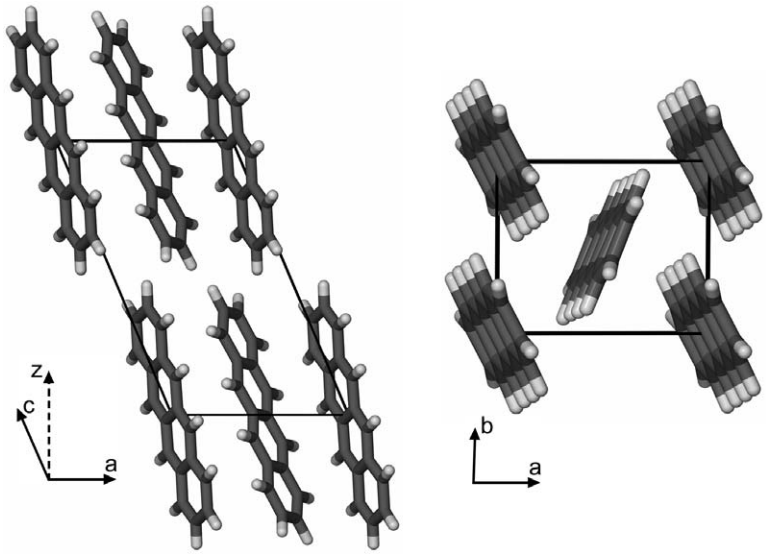

Fig. 1. The triclinic crystal structure of tetracene depicting the stacking of layers in the *z*-direction (left, perpendicular to the *ab* crystal plane) and herringbone arrangement within the layers of the *ab* crystal plane (right). The conduction properties of tetracene depend heavily on the anisotropy of the crystal structure, with significantly faster charge carrier transport within the two-dimensional herringbone layers in comparison to transport between layers (*z*-direction).

and inelastic neutron scattering (INS). Because neutrons can be produced with wavelengths on the order of interatomic distances and energies comparable to those associated with typical harmonic molecular motions, they are ideally suited for probing both structural features and dynamic phenomena in molecular solids. Several particularly useful features of this fundamental property utilized in this investigation. First, owing to the simplicity of the neutron–nuclei interaction, straightforward comparison between experimental and theoretical data is possible. Second, the large incoherent cross-section of hydrogen produces vibrational spectra highly selective to the vibrational modes of the hydrogen nuclei, thereby making INS well suited to probing hydrogenous molecular materials. Third, symmetry based selection rule limitations of optical spectroscopy, causing certain vibrational modes to be "silent", do not apply to inelastic neutron scattering, meaning that all modes are detectable.

Refinement of the neutron powder diffraction, although unable to provide the atomic positions, yielded unit cell parameters for tetracene at 295 K under several pressures. INS data, collected in the 25–75 meV energy range were interpreted using an ab initio calculation on a single, isolated molecule in the gas phase. Over the 0–25 meV range, the vibrational spectra were interpreted through comparison with the results of the ab initio calculation and molecular dynamics simulations. Peak shifts in the vibrational spectra under increasing pressure were assigned to specific intramolecular vibrations or lattice vibrational modes. It is anticipated that the results of this study will aid in deciphering the pressure dependent transport behavior of tetracene and add to understanding of charge conduction in conjugated organic semiconductors.

2. Experimental

2.1. Materials and general procedure

Tetracene ($C_{18}H_{12}$, 98% purity) was obtained from Sigma–Aldrich and used without further purification. Approximately 1.4 g of tetracene was lightly ground to a fine powder, loaded into an aluminum pressure cell of cylindrical geometry, and placed in an orange ILL liquid helium cryostat with a 50 mm diameter sample well. The pressure cell is constructed from a 40 mm diameter cylindrical piece of aluminum and is able to reach a maximum pressure of 400 MPa. The sample compartment is a cylindrical opening 5 mm in diameter and 45 mm long. One end of the cell is sealed using a steel ball and screw mechanism and the other end is connected to the pressure intensifier by a stainless steel capillary. The two-stage piston intensifier system constructed by Harwood Engineering[1] employs a carrier gas, in these experiments helium, to transmit the pressure from the apparatus to the sample. Full details of the pressure apparatus and cell can be found at the NIST Center for Neutron Research website [27].

[1] Trade names or private companies are only mentioned in order to provide complete identification of the relevant experimental details and is not intended as an endorsement by the National Institute of Standards and Technology.

2.2. Neutron powder diffraction

Neutron powder diffraction data were collected using the BT-1 32 detector neutron powder diffractometer at the National Institute of Standards and Technology Center for Neutron Research (NCNR) in Gaithersburg, MD. A Cu(3 1 1) monochromator with a 90° take-off angle, $\lambda = 1.5402(2)$ Å, and in-pile collimation of 15′ were used. Data were collected over the range of 3–168° 2θ with a step size of 0.05° [28]. The diffraction patterns were analyzed with the General Structure Analysis System (GSAS) [29] graphical user interface EXPGUI [30] employing Rietveld refinement of the unit cell parameters in the 5–36° and 46–55° 2θ range. The 36–46° range of the diffraction patterns are excluded from the structural analysis because diffraction in this region is dominated by two large aluminum diffraction peaks representing the (0 0 1) and (1 1 1) crystal planes of the pressure cell. The initial conditions used to refine the diffraction data at atmospheric pressure were obtained from the crystal structure and atomic positions given in the TETCEN structure of the Cambridge Structural Database (space group $= P\bar{1}$; $a = 7.90$; $b = 6.03$; $c = 13.53$; $\alpha = 100.3$; $\beta = 113.20$; $\gamma = 86.30$) [31]. At all other pressures, the initial refinement parameters were the final results obtained in refining the diffraction data of the next lower pressure.

2.3. Inelastic neutron scattering

INS spectra, representing the intensity of scattered neutrons as a function of energy transfer, were collected up to 75 meV (600 cm^{-1}) using two instruments located at the NIST Center for Neutron Research. Between 25 and 75 meV (200 and 600 cm^{-1}) the data were collected using the filter analyzer spectrometer (FANS) located on beam tube BT-4 [32]. The incident neutron beam collimated to 20/10′ divergence, yielding an instrumental resolution of approximately 1.1 meV (~9 cm^{-1}). Although the FANS instrument is able to collect data up to 220 meV (1760 cm^{-1}), the spectra of tetracene up to 75 meV contained sufficient peaks indicative of intramolecular vibrations to assess the pressure dependence on the vibrational dynamics that are primarily dictated by internal molecular geometry and bonding.

The spectra between 0 and 25 meV (0 and 200 cm^{-1}) were collected with the Fermi Chopper time-of-flight (TOF) spectrometer on neutron guide NG-6 [33]. The TOF data were collected using monochromatic neutrons with wavelength of 4.8 Å. In this configuration, the TOF instrument has an energy resolution of less than 0.5 meV (~4 cm^{-1}) over the experimental energy range. For both instruments, the sample spectra were corrected for back-

ground scattering by subtracting the spectrum obtained from the empty pressure cell under identical conditions.

2.4. Ab initio calculations

The harmonic vibrational mode frequencies of tetracene were determined from ab initio calculations using density-functional theory in a manner similar to the tetracene analyses performed previously [26,34–36]. These calculations were executed on a single, isolated tetracene molecule using the *Gaussian98* program module contained in the Cerius[2] software package employing the B3LYP density functional approximation and 6-31-G* basis set [37]. A "theoretical" spectrum for direct comparison with the experimental INS data was generated by calculating the relative intensity expected at each vibrational mode frequency. As part of this analysis, account was taken of the relative neutron scattering cross-sections and atomic displacements, spectral broadening based on instrument parameters, and an appropriate Debye–Waller factor similar to that previously used to simulate spectra for the linear polyacene molecules naphthalene and anthracene [38]. The calculated vibrational frequencies were not scaled in this analysis, which is common for comparison of ab initio calculations with IR and Raman spectra. From these results, it was possible to assign all of the experimental spectral features in the data collected using the FANS instrument over 25–75 meV to specific intramolecular vibrational modes of the tetracene molecule.

2.5. Molecular dynamics simulations

In order to appropriately model the lattice vibrational modes MD simulations were performed at 1 atm and 358 MPa on a crystalline system consisting of 5 herringbone layers with 180 molecules per layer. The complete representative crystal containing 900 tetracene molecules and 27,000 atoms was constructed from the atomic coordinates given in the TETCEN crystal structure [31]. Simulations with smaller numbers of atoms often resulted in structural changes that were attributed to finite-size effects. Force-field parameters were derived for the CHARMM-27 analytical potentials and atom types [39]. Gaussian03 [40] was used to calculate equilibrium bond lengths and angles from for an isolated tetracene molecule from the crystal structure using ground state Hartree–Fock using the 6-31G* basis set. Atomic point charges were calculated using the RESP methodology [41]. In order to obtain agreement with experiment in the low energy (<25 meV) range, C–C–H–C and C–C–C–C improper torsion potentials (80 kcal/mol/rad^2) were required. Three-dimensional periodic boundary conditions were used and electrostatic potential energies were calculated using the smooth particle mesh Ewald sum [42]. Lennard-Jones interactions and the real space part of the Ewald sum were smoothly truncated at 14 Å (switching from 10 Å). The Nosé-Hoover chain method was used to control temperature [43] and pressure [44] using a fully flexible simulation box with multiple-time step integrators [45] implemented in the program PINY_MD [46]. The system was simulated for 700 ps at each condition where the last 200 ps were used for analysis (time step = 1 fs). Low energy spectra were calculated from the Fourier transform of the velocity autocorrelation function of hydrogen atoms [47].

3. Results and discussion

3.1. Neutron powder diffraction

The experimental data and fit results of the neutron powder diffraction pattern from tetracene at atmospheric pressure are provided in Fig. 2. Peaks observed in the diffraction data result from constructive interference between coherent, elastically scattered neutrons. Due to the thickness of the pressure cell, the intensity of coherently diffracted neutrons from the aluminum pressure cell was much greater than from the tetracene sample (see inset, Fig. 2). In order to facilitate refinement of the structural parameters corresponding solely to tetracene, the large contributions to the diffraction pattern between 2θ of 36° and 46° from the aluminum pressure cell were excluded from the range of data fit during analysis. Owing to the large *incoherent* scattering cross-section of hydrogen (80.26 barns) in comparison with to the *coherent* scattering cross-sections of carbon (1.757 barns) and hydrogen (5.551 barns), the diffraction patterns have a large background intensity of inelastically scattered neutrons. This background scattering contributes noise to the data, resulting in a incoherent to coherent signal ratio that increases as a function of 2θ such that the diffraction data at 2θ greater than 55° does not exhibit discernable diffraction peaks suitable for the fitting analysis.

The neutron powder diffraction data collected at atmospheric pressure is qualitatively similar to the data collected

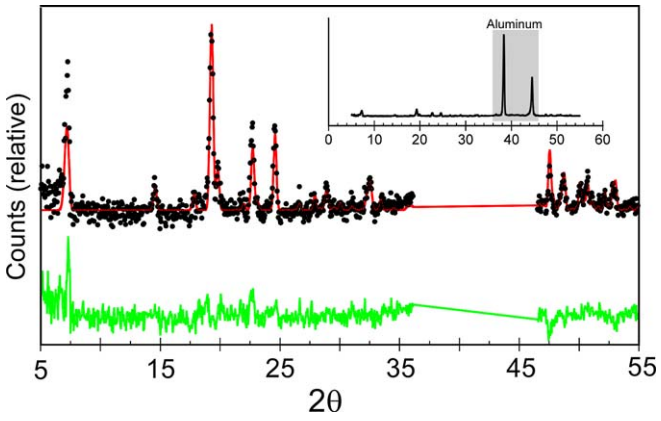

Fig. 2. Background subtracted powder diffraction data (closed circles), fit (solid line), and residual difference between the fit and data (bottom gray line). The 2θ range between 36° and 46° has been excluded from the fitting protocol as it contains two large peaks from the aluminum sample cell (see inset).

at all pressures. For each diffraction pattern, the 2θ values and intensity of the fit pattern are in reasonable agreement with the experimental data. The intensity of the peak at $2\theta \approx 7°$, corresponding to reflections from the (0 0 1) crystal plane, are systematically underestimated by the fit. This discrepancy may result from the plate-like morphology of the crystals causing them to align in a preferred orientation of the within the sample container, thereby skewing the diffracted intensity from that of an isotropic sample.

Since only the first 15 peaks in the experimental data were available for refinement, it was not possible to obtain the atomic coordinates of each molecule in the asymmetric unit cell using Rietveld analysis. The unit cell parameters, however, were obtained and are given in Table 1 as a function of pressure. As expected, the overall volume of the unit cell decreases with increasing pressure, decreasing from a value of 576 Å^3 at atmospheric pressure to 557 Å^3 at 358 MPa corresponding to an overall change of 3.3%. This change in volume is nearly half of that observed for anthracene under similar pressure [48], indicating an increased bulk modulus with the addition of a single fused acene ring. Further, the unit cell volume at 295 K and 358 MPa of 557 Å^3 for tetracene is in close agreement with the 550 Å^3 value obtained at 140 K and atmospheric pressure in a previous X-ray diffraction investigation of tetracene as a function of temperature [49]. Additionally, within the *ab*-plane, the percent decrease in area is 2.5% at 358 MPa. This value may prove important in explaining pressure-induced conductivity enhancement within these and similar materials.

Changes to the unit cell length and angle parameters of tetracene as a function of increasing pressure are depicted in Fig. 3. Between atmospheric pressure and 358 MPa the percent contraction of the unit cell *a* parameter is 1.6% with the *b* and *c* parameters each decreasing by 1.1%. While

Table 1
The unit cell parameters of tetracene as a function of pressure at 295 K determined in this study and as a function of temperature at atmospheric pressure from Ref. [49]

Cell parameters	Tetracene refinement results at each pressure, 295 K					Ref. [49], 1 atm	
	1 atm	92.5 MPa	218 MPa	286 MPa	358 MPa	293 K	140 K
a (Å)	7.872(22)	7.871(24)	7.820(22)	7.775(18)	7.747(14)	7.915(5)	7.74(4)
b (Å)	6.055(9)	6.052(10)	6.030(8)	6.009(12)	5.987(7)	6.065(2)	5.99(2)
c (Å)	13.42(9)	13.40(10)	13.40(10)	13.36(12)	13.27(9)	13.445(12)	13.20(10)
α	101.10(11)	101.26(21)	101.23(9)	100.39(19)	100.15(7)	101.10(6)	102.4(5)
β	113.39(30)	113.38(35)	113.54(28)	113.27(31)	113.16(15)	113.31(9)	113.8(9)
γ	85.94(8)	85.84(9)	85.87(8)	86.04(10)	86.14(4)	85.91(4)	86.0(4)
V (Å^3)	576	574	568	564	557	582	550
$ab\sin\gamma$ (Å^2)	47.5	47.5	47.0	46.6	46.3	47.9	46.2
z (Å)	12.08(13)	12.06(11)	12.04(25)	12.06(27)	12.02(12)	12.11	12.04

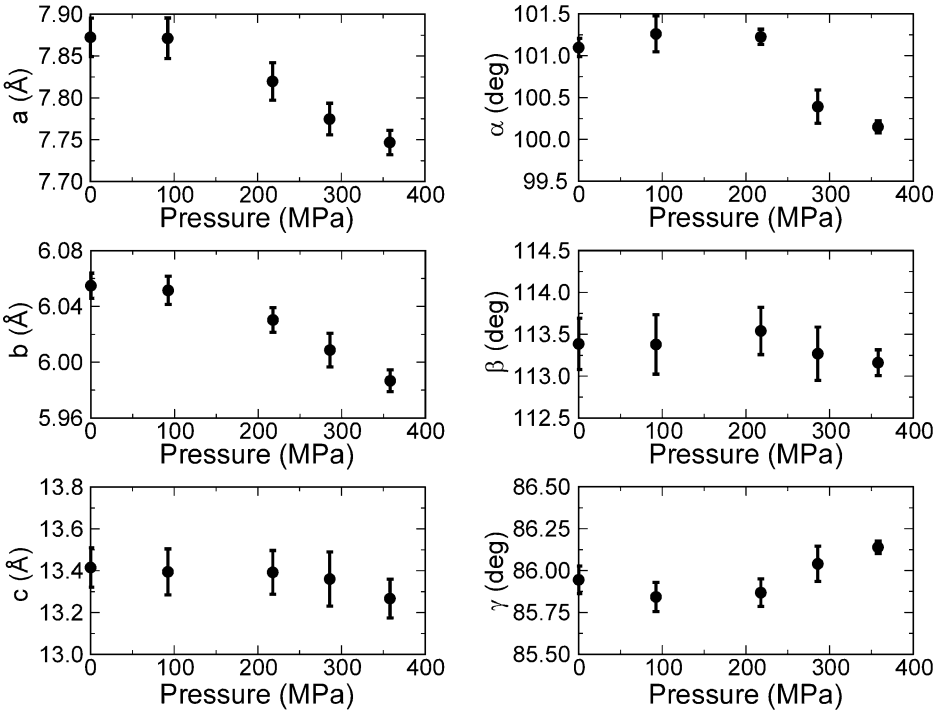

Fig. 3. The unit cell parameters of tetracene as a function of pressure at 295 K obtained by fitting the experimental neutron powder diffraction data.

the total contraction observed with regard to each unit cell length is of relatively the same magnitude, the pressure dependent behavior differs. A continuous decrease over the entire pressure range is apparent for the unit cell lengths associated with the a and b unit cell parameters, whereas the c parameter remains nearly constant up to the measurement at 286 MPa with a slight decrease at 358 MPa. When comparing the unit cell length parameters with those measured at 293 and 140 K (see Table 1) [49], structural modifications of similar magnitude are observed with the application of external pressure as with cooling. In the pressure range measured, the compressibility along the a, b, and c-directions are -3.8×10^{-4}, -1.9×10^{-4}, and -3.4×10^{-4} Å/MPa, respectively. Interesting, however, is the relatively small change observed in the z parameter in Table 1. The z parameter is a measure of the vertical distance between ab crystal planes, indicative of the interlayer stacking distance. The compressibility in the z-direction over the full pressure range is -1.2×10^{-4} Å/MPa. For the most part z remains nearly constant within the precision of the measurement. Thus, despite relatively large molecular rearrangements within the crystal, the interlayer distance between herringbone planes is maintained.

Angles defining the relative orientation of the triclinic unit cell appear to remain nearly constant (within experimental error) from atmospheric pressure up to the measurement at 218 MPa. At the two measured pressures above 218 MPa, α decreases, β decreases slightly, and γ increases. As opposed to the unit cell length parameters, these angles do not follow a similar trend with that observed in tetracene crystals cooled to 140 K [49]. Rather, at pressures greater than 218 MPa, α and β both display behavior opposite that observed in the temperature investigation. Additionally, γ increases to a much greater extent than with cooling.

In general, the pressure dependent behavior of the unit cell parameters of tetracene parallels the experimental results from X-ray diffraction data collected on related aromatic molecules of anthracene [48,50] and polyphenylenes [51,52]. Because these molecules have crystal structures adopting a layered, herringbone motif packing arrangement similar to that of tetracene, interpretation of the neutron diffraction results here follows the discussion of those previous investigations. Disproportionate decrease in the a unit cell length as compared with the b parameter in parallel with the distinct increase in γ at pressures between 218 and 286 MPa indicates a structural modification that causes a flattening of the herring bone pattern, meaning the edge-on-face orientation is converting to a more pseudo-dimeric π-stacked structure. Compression in the c-direction causes the long axis of the tetracene molecule to tilt further out of alignment with the z-direction. These qualitative conclusions are supported by corresponding fluorescence measurements collected on tetracene as a function of pressure indicating relative flattening of the herringbone angle by 15° and greater tilting with respect to the ab layers by ~6° to 9° [25].

3.2. Inelastic neutron scattering and ab initio calculation of tetracene intramolecular vibrational modes in the 25–75 meV energy range

The experimental INS spectra of tetracene between 25 and 75 meV obtained at 295 and 100 K under ambient pressure using the filter analyzer spectrometer (FANS) are shown in Fig. 4. Differences between the overall features contained in each spectrum are slight. The lower temperature spectrum, however, displays shifts to higher energy in some of the spectral peaks and possesses sharper, better-resolved peaks owing to less thermal motion in the sample. One discernable difference between the spectra is the peak observed at approximately 62 meV that is clearly apparent in the 100 K spectrum, but poorly resolved at 295 K. The small peak apparent in both spectra at 51 meV is due to vibration of the beryllium instrument filter, not the sample. Overall, the spectra contain several apparent peaks, each corresponding to the energy of intramolecular vibrational modes of the tetracene molecules.

Also included in Fig. 4 is a theoretical spectrum constructed from the results of an ab initio density functional theory calculation performed on a single, gas-phase tetracene molecule using the Gaussian98 program [37]. The vertical bars on the bottom of the graph depict the frequency and relative intensity of the predicted vibrational modes, regardless of vibrational symmetry, which were used to construct the theoretical spectrum. On the whole the theoretical spectrum replicates, the features of the experimental spectra collected using the FANS instrument remarkably well in terms of both the intensity and energy of the spectral features. A noticeable distinction between the experimental and theoretical spectra are the relative intensity of

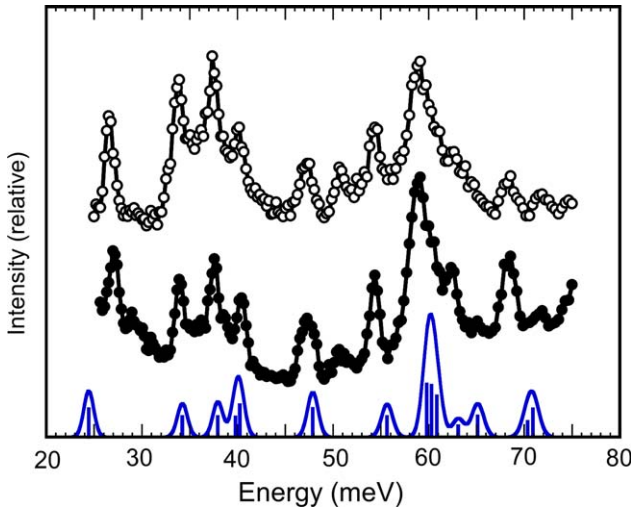

Fig. 4. Experimental INS spectra of tetracene collected on the FANS instrument at 100 K (●) and 295 K (○) at ambient pressure and the density-functional theory calculated spectrum (solid line) in the 25–75 meV energy range. The vertical lines represent the energy and relative intensity of the theoretically calculated vibrational modes used to construct the theoretical spectrum.

the peak at ~40 meV and the slightly higher energy predicted by the theoretical calculation for the experimental peaks at ~62 and ~68 meV. The overall similarity between the features of the experimental data and the theoretical prediction, however, is adequate to draw reliable correlations between the spectra. Since the ab initio calculation is unable to account for intermolecular lattice phonon modes, the ability of the single molecule gas phase calculation to account for all of the experimental features over the 25–75 meV energy range indicates that the peaks observed in the data are due exclusively to intramolecular vibrations that do not appear to be affected by any increase in density of the crystal structure with cooling. Because only intramolecular vibrations are involved over this energy range, changes in the vibrational behavior with cooling indicate the effect of increasing steric intermolecular interactions on the internal vibrations – governed by the molecular geometry and covalent bonding. As a result, changes to these spectra from a phase transition would only be apparent when the resulting changes to the intermolecular orientations caused relatively large modifications to the intermolecular energetics causing them to achieve magnitudes comparable with the intramolecular covalent bonds. Changes to the vibrational energies due to the reported phase transition at 170 K [24], therefore, are most likely not discernable in the spectra.

Quantitative comparison between the INS spectra collected on the FANS instrument and that of the theoretical calculation over 25–75 meV is given in Table 2. Each peak in the experimental spectra was fit by a Gaussian line-shape of variable width to obtain the peak energy. Inspection of the changes to the experimental peak energies as a function of cooling indicates some peaks are more strongly affected by cooling than others. The peaks measured at 26.6 and 40.1 meV at 295 K display the largest shifts with respect to cooling by shifting by 0.5 and 0.4 meV, respectively, with the 195 K temperature decrease to 100 K. Furthermore, as is apparent from comparison between the theoretical and experimental spectra collected at 100 K, the experimental peaks at ~27.1, 34.0, 37.6, 47.4, and 54.3 meV each result from a single, non-overlapping vibrational mode. The remaining peaks, at 40.5, 59.0, 62.5, and 68.4 meV, are due to the overlap of multiple vibrational modes.

Table 2
Experimental peak and theoretically determined vibrational mode energies of tetracene, corresponding to peaks observed in the INS spectra between 25 and 75 meV collected under ambient pressure (1 atm) at 100 and 295 K using the FANS instrument

Peak	100 K	295 K	Ab initio calculation	
	E (meV)	E (meV)	E (meV)	Intensity
6	27.1	26.6	24.4	0.61
7	34.0	33.7	34.2	0.47
8	37.6	37.5	37.9	0.52
9	40.5	40.1	39.8	0.37
			40.2	0.60
10	47.4	47.2	47.9	0.72
11	54.3	54.4	55.6	0.57
12	59.0	59.0	59.9	1.00
			60.2	0.97
			60.9	0.77
13	62.5	62.5	63.1	0.35
			65.1	0.65
14	68.4	68.2	70.4	0.37
			71.0	0.68

Schematic illustrations of the atomic displacements corresponding to all ab initio calculated intramolecular vibrational modes of tetracene between 0 and 75 meV are provided in Fig. 5. From these illustrations and the correlation between experimental and theoretical spectra provided in Fig. 4 and Table 2, the atomic displacements of distinct intramolecular vibrational modes can be assigned to the spectral peaks in a rather straightforward manner. The vibrational modes can be classified into two generic categories relative to the plane defined by the aromatic rings of the molecule. Vibrations with atomic displacements parallel to the plane of the tetracene molecule occur at 20.4, 37.9, 39.8, 55.6, 63.1 and 71.0 meV (illustrated as face-on in Fig. 5). The vibrational modes at 7.1, 11.5, 19.0, 40.2, 47.9, 59.9, 60.2, 60.9, 65.1, and 70.4 meV correspond to atomic displacements perpendicular to the plane of the tetracene molecules (illustrated as edge-on in Fig. 5).

Fig. 6 depicts the INS spectra of tetracene collected as a function of pressure over the 25–75 meV energy range at 100 and 295 K. At 295 K the spectra are shown for pressures of 1 atm, 218 MPa and 358 MPa; whereas, at 100 K only the spectra at 1 atm and 358 MPa are shown. The pressure-induced changes to the spectra observed at both 100 and 295 K display similar behavior despite the difference in temperature. As such, these results support the conclusion that cooling and pressure appear to have a similar affect on the intramolecular vibrations within the experimental temperature and pressure ranges. Inspection of the spectral changes with increasing pressure indicates that the peaks in the 295 K spectra at roughly 26, 34, 40, 47, and 59 meV are shifted to higher energy; whereas, the remaining peaks near 37, 54 and 68 meV appear unchanged by the increase in pressure. The shoulder observable at 62.5 meV at 1 atm and 295 K also appears unchanged by compression of the crystal lattice.

An overall summary of the peak positions corresponding to molecular motions of tetracene as a function of pressure at 295 K is provided in Table 3. Each peak observed in the 25–75 meV energy range collected with the FANS instrument is listed for several pressures between atmospheric and 358 MPa. The listed peak energy was obtained by individually fitting the experimental peaks with a Gaussian line-shape of variable width, with the peak energy recorded as the location of the center of the Gaussian curve. Peak numbers were assigned similar to Table 2. The peak list begins with peak 6 since, as will be shown below, the low energy spectrum between 0 and 25 meV contains the peaks designated 1–5. Unfortunately, the peak observed at 62.5 meV could not be sufficiently resolved at

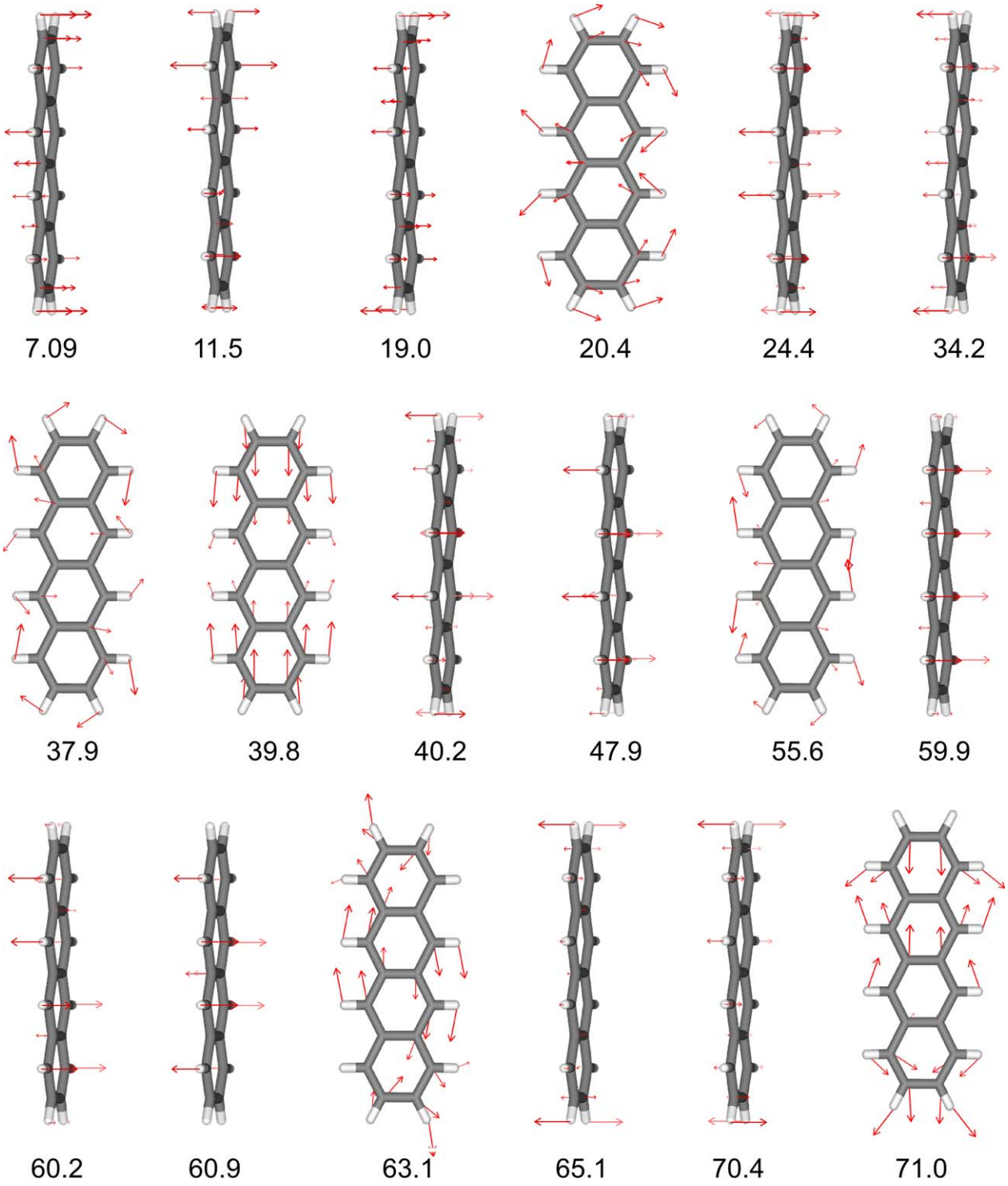

Fig. 5. Schematic representation of the atomic displacements of the theoretically calculated vibrational modes of tetracene between 5 and 75 meV as determined by ab initio calculation. The relative magnitudes of the arrows correspond to the atomic displacement in one-quarter of the overall vibration. Energies are provided in units of meV (1 meV $\approx$ 8 cm^{-1}).

any pressure other than 1 atm to be able to provide that peak's energy at elevated pressures.

Quantitative analysis of the influence of increasing pressure on the energetics of tetracene is possible by inspection of the magnitude of the peak shift as a function of pressure represented by the value Δ. The magnitude of the peak shift for an individual peak was ascertained by a linear fit of the peak center as a function of pressure. The greater the value of Δ, the more a peak is shifted to higher energy with increasing pressure. As such, those vibrational modes most significantly affected by compression of the crystal lattice have larger values of Δ. To facilitate comparison of these

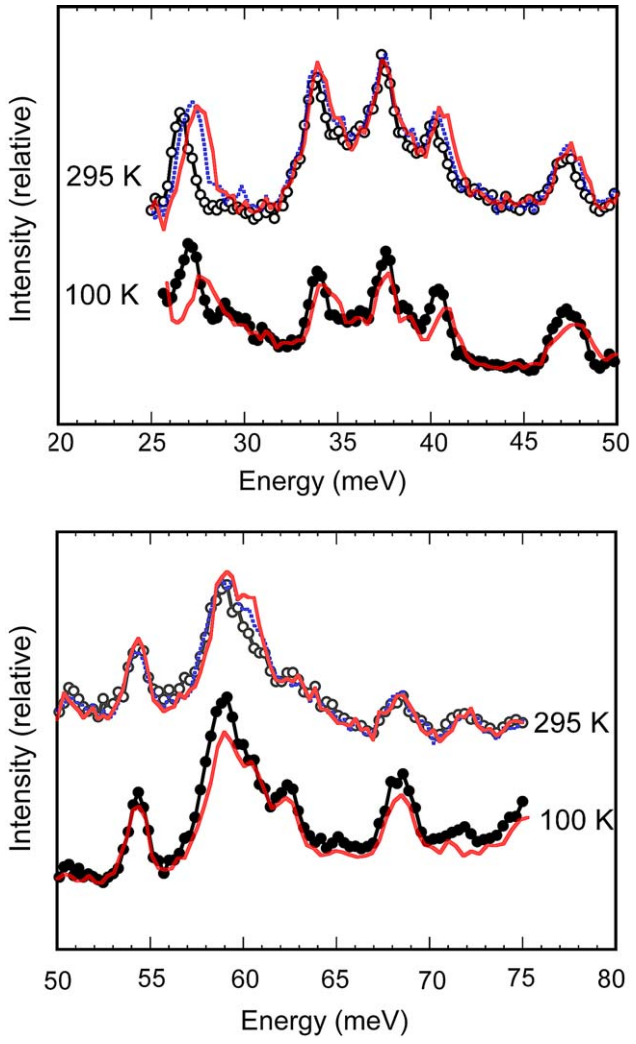

Fig. 6. Ambient and high pressure experimental INS spectra of tetracene collected using the FANS instrument at 295 K (top) and 100 K (bottom). The ambient pressure data are depicted by open circles (○) at 295 K and filled circles (●) and 100 K. The spectra collected at 218 and 358 MPa are indicated by the dashed line (295 K only) and solid lines, respectively.

results with the vibrational modes depicted in Fig. 5, the table also contains a column representing the relative atomic displacement, either parallel (∥) or perpendicular (⊥) to the molecular plane, of the vibrational modes assigned to the experimental peaks.

Examination of the magnitude of the peak shifts with respect to pressure and the relative atomic displacement indicates application of pressure has an anisotropic effect on the intramolecular vibrational modes of tetracene. The peaks observed at 37.5 and 54.3 meV at 1 atm, the only peaks consisting solely of motions parallel to plane of the molecule, display negligible changes with increasing pressure up to 358 MPa. All remaining spectral peaks contain vibrational modes with atomic displacements perpendicular to the molecular plane and demonstrate pressure dependent increases in energy. In addition to the anisotropy, one would expect a greater change to the intramolecular vibrational modes at lower energy since these modes would tend to be more strongly affected by an increase in steric intermolecular interactions caused by compression of the crystal lattice [53]. Overall, the results between 25 and 75 meV support a conclusion that intramolecular vibrational modes perpendicular to the plane of the molecule represent the only vibrations that are significantly affected by increasing pressure to 358 MPa.

3.3. Inelastic neutron scattering and molecular dynamics simulation of tetracene intramolecular vibrational and lattice phonon modes in the 0–25 meV energy range

Low energy spectra collected between 0 and 25 meV energy transfer on tetracene at 100 and 295 K under ambient pressure using the time-of-flight (TOF) instrument are shown in Fig. 7. It should be noted that the TOF instrument measures the energy transferred from a molecular vibration to an incident neutron; hence, the abscissa of plots for this instrument are given in negative energies. This instrumental feature merely represents a sign change in the vibrational spectra that is of no account to a full description of the low energy dynamics. Because the TOF instrument is fairly sensitive to the thermal energy of the sample, the peaks of the low temperature spectrum are much sharper than at 295 K. Additionally, the 100 K data are systematically shifted to slightly higher energy due to compression

Table 3
Peak energies observed in the experimental INS spectra of tetracene between 25 and 75 meV at 295 K under increasing pressures

Peak	1 atm	108 MPa	223 MPa	299 MPa	358 MPa	$\Delta \times 10^3$ (meV/MPa)	Ab initio atomic displacement
	(meV)	E (meV)	E (meV)	E (meV)	E (meV)		
6	26.6	26.8	27.1	27.3	27.4	2.4 (0.1)	⊥
7	33.7	33.7	33.9	34.0	34.0	0.9 (0.2)	⊥
8	37.5	37.5	37.5	37.5	37.5	0.1 (0.1)	∥
9	40.1	40.4	40.4	40.6	40.7	1.5 (0.2)	∥ & ⊥
10	47.2	47.2	47.2	47.3	47.5	0.7 (0.3)	⊥
11	54.3	54.3	54.2	54.3	54.3	~0 (0.1)	∥
12	59.0	59.2	59.2	59.2	59.4	0.9 (0.2)	⊥
13	62.5	–	–	–	–	–	∥ & ⊥
14	68.2	68.2	68.3	68.3	68.3	0.3 (0.2)	∥ & ⊥

The peak shift (Δ) is quantified as the slope obtained by fitting the peak energy as a function of pressure to a straight line with the uncertainty in slope given in parentheses. The relative atomic displacement of the vibrational modes responsible for the spectral peak were assigned from the ab initio calculation and atomic trajectories provided in Fig. 5 and designated as perpendicular (⊥) or parallel (∥) to the molecular plane.

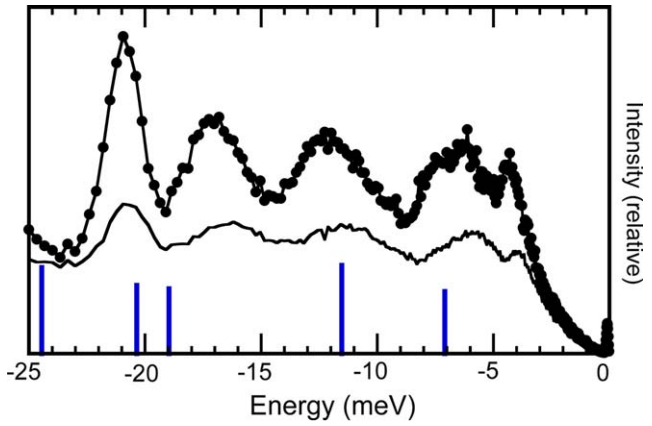

Fig. 7. Experimental INS spectra of tetracene collected on the TOF instrument at 100 K (●) and 295 K (solid line only) at ambient pressure along with the energy and relative intensity of the ab initio calculated intramolecular vibrational modes (vertical lines) obtained from the density-functional theory calculation in the 0–25 meV energy range.

Table 4
Experimental peak and theoretically determined vibrational mode energies of tetracene, corresponding to peaks observed in the INS spectra between 0 and 30 meV from data collected using the FCS instrument

Peak	100 K	295 K	Ab initio calculation	
	E (meV)	E (meV)	E (meV)	Intensity
1	4.2	3.7		
2	6.6	5.9		
			7.09[a]	0.44
3	12.2	11.3		
			11.53[a]	0.63
4	17.3	16.6		
5	20.9	20.9	18.97	0.46
			20.36	0.49

[a] While these calculated vibrational energies cannot be directly assigned to any particular spectral peak, they have been included in this table for completeness.

of the crystal lattice upon cooling (see Table 4). Other than the change in peak sharpness and shift to slightly higher energy, however, the similar features of both spectra indicate the low energy spectra are not particularly sensitive to any phase transition upon lowering temperature. The inability to detect changes in the lattice modes from the phase transition is likely due to the modest changes in the molecular orientation of the crystal structure associated with the transition that result in subtle changes to the spectrum that cannot be discerned from the broad dispersion contained in the peaks. Such result is not surprising because INS measures the vibrational energies at all points within the crystal and subtle changes to the molecular orientations may not significantly alter the full dispersion of the vibrations so as to be distinguishable in the INS spectra. Raman scattering, on the other hand, is sensitive to these subtle changes in the low energy vibrations because it measures the vibrational energy at only one point in the lattice, at the zone center.

The TOF spectra at 100 and 295 K indicate 5 total peaks: a small peak at ~4 meV, three broad peaks between 5 and 19 meV, and a relatively strong intensity peak at ~21 meV. The breadth of these peaks is due to strong phonon dispersion across the Brillouin zone at low energy and overlapping contributions of multiple vibrational modes. Since INS measures the vibrational energies at all points within the crystal, peaks in the INS spectra tend to be centered at a median energy representing a "zone-averaged" energy, whether at the zone center or otherwise. The peak shape of the INS spectrum is the result of the particular dispersion associated with the vibration responsible for the peak. As opposed to vibrational modes at higher energies that tend to have little dispersion, discrepancies between experimental peaks observed in both Raman and INS at low energies are often attributable to whether the technique is sensitive to dispersion. Such differences between the techniques can account for the differences in the spectra of this study and that of a previous Raman investigation of tetracene [26].

The energy and intensity of the ab initio calculated intramolecular vibrational modes up to 25 meV are also graphically depicted in Fig. 7 and provided in Table 4 for comparison with the experimental measurements. While the validity of a calculation that does not account for the crystal lattice is questionable since low energy lattice phonon modes occur in this energy range, the four theoretical intramolecular ab initio modes found in this study are nearly identical to those obtained by lattice-dynamical calculations performed on "rigid" tetracene molecules [53]. More specifically, the experimental peak at ~21 meV can be assigned to an overlap of the two theoretical intramolecular modes calculated at 19.0 and 20.4 meV. The slight underestimation of the energy of these two vibrational modes by the ab initio calculation is either the result of dispersion toward higher energy in the modes unaccounted for by the calculation or a change in the energetics induced by intermolecular forces from the adjacent molecules of the crystal causing the peak to shift to an energy higher than predicted. A similar result is observed in Raman experiments at 21.02 meV [53]. The similarity in energy between the Raman and INS measurements implies little dispersion in the energy of these vibrations. Yet, due to the symmetry based selectivity rules of optical spectroscopy, contributions to this Raman observed feature is solely due to vibration of A_g symmetry calculated at 19.0 meV. Contribution from the calculated mode at 20.4 meV, which adds to the intensity of the INS spectral peak, is not present in the Raman scattering since the vibration has A_u symmetry. The peak thus contains one parallel and one perpendicular mode in relation to the molecular plane (see Fig. 5). The accuracy of the energy calculated for the two lowest perpendicular intramolecular modes at 7.10 and 11.5 meV is questionable since low energy modes are typically more sensitive to intermolecular forces than those possessing higher energies. Most likely, these intramolecular modes contribute intensity to the low energy spectra but mix significantly with lattice phonon modes and, hence,

cannot be explicitly assigned to any spectral peaks [26]. Similar results have been observed previously for the low energy vibrational modes of other polyacenes including anthracene [54] and pentacene [55].

In order to get beyond the limitations inherent in the ab initio calculation, we performed molecular dynamics simulations on a sufficiently large construction of the crystal structure such that it was possible to model the full low energy spectra collected on tetracene using the TOF instrument. The MD simulations include dynamic contributions from both intramolecular vibrations and lattice phonon modes and should, therefore, account for all molecular motions that occur. Additionally, because the crystal structure is included in the simulation it is possible to calculate directly the low energy vibrational behavior at elevated pressure, which is not possible in the ab initio calculations. As a check on the validity of the modeled crystal structures, the unit cell parameters of the equilibrated structures at both 1 atm and 358 MPa were compared with the unit cell parameters from the neutron powder diffraction (Table 5). Overall, the MD equilibrated structures conform reasonably well with the experimental results with a difference of 5% between the simulated and measured unit cell volumes and a correspondence in each of the unit cell parameters greater than 98% at 1 atm and 97% at 358 MPa.

Fig. 8 contains the experimental INS spectra collected at 1 atm and 358 MPa and 295 K and compares them with the results of the molecular dynamics simulations under identical conditions. The energy of the five distinct peaks observed in the experimental TOF data at several pressures between 1 atm and 358 MPa are listed in Table 6. It should be mentioned that the peak shifts collected in the table are nearly linear for each peak over the full pressure range. Examining the magnitude of the peak shifts with pressure shows that not all peaks are similarly affected by increasing pressure. Specifically, the experimental peaks apparent at approximately 12 and 17 meV exhibit relatively large shifts to higher energy whereas, the roughly 4, 6 and 21 meV peaks display significantly less of this behavior.

Inspection of Fig. 8 reveals remarkable overall qualitative agreement between the energy and relative intensity

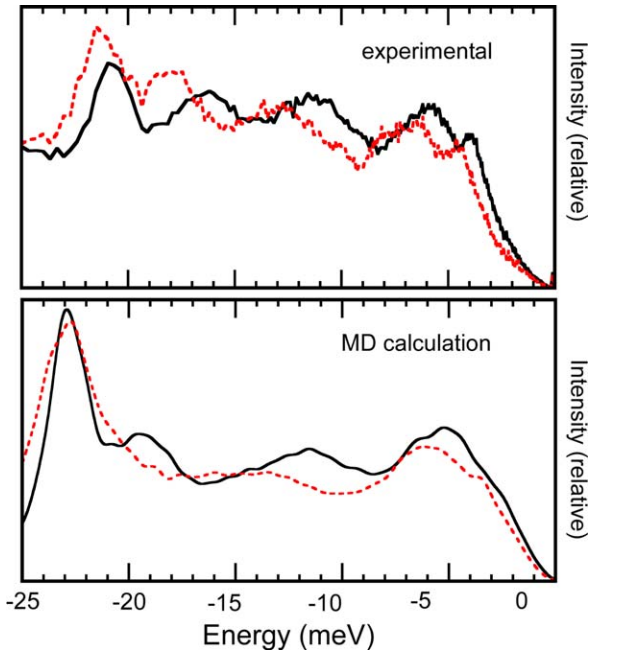

Fig. 8. Comparison between the experimental INS spectra collected using the TOF instrument and molecular dynamics calculated spectra at 295 K under ambient pressure (solid line) and at 358 MPa (dashed line) over the 0–25 meV energy range.

of the features contained in the experimental and simulated spectra at both 1 atm and 358 MPa. Such straightforward similarity promotes confidence in the validity of the molecular dynamics results. In fact, both methods indicate identical shift in the spectra with energy. For instance, the 1 atm results of the MD simulation show a very slight kink in the spectra at around 3 meV and four broad peaks centered at approximately 5, 12, 19, and 23 meV. These features match the peaks contained in the experimental spectra at 3.7, 5.9, 11.3, 16.6 and 20.9, respectively. At 358 MPa, the correlation between the experimental and simulated spectra is comparable with that at 1 atm with two exceptions. First, the kink in the MD spectrum corresponding to the lowest energy experimental peak at 4.2 meV at 358 MPa is more discernable. Second, the feature in the MD spectrum corresponding to the 18.0 meV experimental peak appears as a low energy shoulder on the much more intense peak at ~23 meV.

Deconvolution of the overall powder-averaged low energy MD spectra at 1 atm and 358 MPa (Fig. 8) into contributions from motions within the *ab*-plane of the herringbone layers and the *z*-direction perpendicular to the herringbone layers are provided in Fig. 9. Overall, the in-layer spectra display several features across the full energy range up to 25 meV. The *z*-direction spectra, on the other hand, only display two broad peak-like features that are concentrated to two distinct energy ranges. The lowest energy features, which correspond to phonon acoustical modes, in the *z*-direction is a few meV lower than in the layer. It appears, therefore, that the lowest energy peak observed in the experimental spectra at roughly 4 meV is

Table 5
Optimized unit cell parameters and percent difference with the neutron powder diffraction results of the molecular dynamics energy minimized structures of tetracene at 1 atm and 358 MPa

Cell parameters	1 atm	% Difference, 1 atm	358 MPa	% Difference, 358 MPa
a (Å)	8.02	1.88	7.93	2.37
b (Å)	6.17	1.90	6.10	1.89
c (Å)	13.67	1.90	13.52	1.91
α	102.53	1.42	102.53	2.38
β	113.39	~0	113.38	0.19
γ	85.94	~0	85.94	−0.23
V (Å^3)	606.27	5.27	586.45	5.32
$ab\sin\gamma$ (Å^2)	49.36	3.92	48.25	4.21
Z (Å)	12.25	1.41	12.11	0.75

Table 6
Peak energies observed in the experimental INS spectra of tetracene between 0 and 25 meV at 295 K under increasing pressures

Peak	1 atm	108 MPa	223 MPa	299 MPa	358 MPa	$\Delta \times 10^3$ (meV/MPa)	Ab initio atomic displacement
	(meV)	E (meV)	E (meV)	E (meV)	E (meV)		
1	3.7	3.9	4.1	4.2	4.2	1.5 (0.1)	
2	5.9	6.1	6.3	6.5	6.6	1.9 (0.1)	⊥
3	11.3	11.9	12.6	12.8	13.1	4.9 (0.4)	⊥
4	16.6	17.3	17.6	17.9	18.0	3.9 (0.4)	
5	20.9	21.1	21.2	21.3	21.4	1.3 (0.1)	∥ & ⊥

The magnitude (Δ) and uncertainty (in parentheses) of the peak shift is the slope obtained by fitting the peak energy as a function of pressure to a straight line.

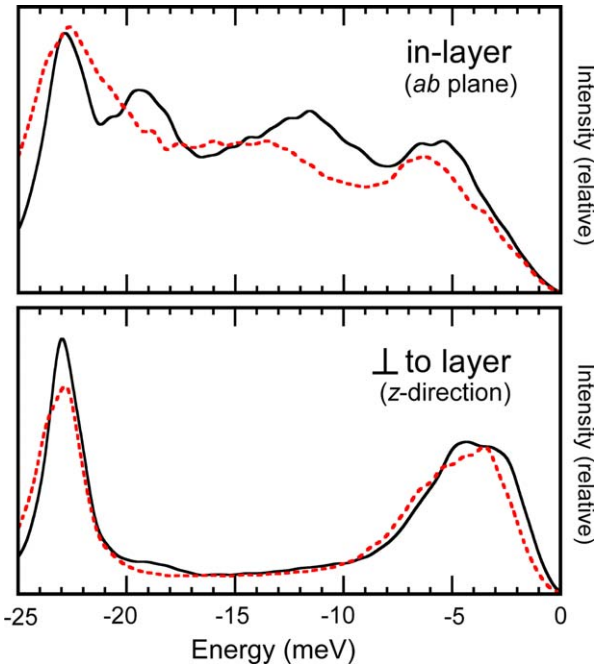

Fig. 9. Comparison of the MD calculated spectra for tetracene at 1 atm (solid line) and 358 MPa (dashed line) for vibrational motions occurring within the herringbone layer (in the *ab*-plane of the unit cell) and projected along the *z*-direction perpendicular to the herringbone layers.

the result of the phonon acoustical mode in the *z*-direction. The experimental peaks near 6 and 21 meV contain contributions from molecular motions both within and perpendicular to the herringbone layer. This observation for the peak at 21 meV is consistent with the assignment of the peak to two intramolecular vibrational modes – one with atomic displacements entirely within the *ab*-plane, the other with displacements both in the *ab*-plane and *z*-direction. The experimental peaks at 1 atm observed at 11.3 and 16.6 meV are strictly due to vibrational modes that occur within the *ab*-plane.

A main distinguishing feature between the *ab*-plane and *z*-direction spectra is the significant shift to higher energy of the in-layer spectra, compared with the minimal change to the perpendicular-to-layer spectra, with increasing pressure. In fact, the large shift in the experimental peaks at 12 and 17 meV with increasing pressure are reproduced extremely well in the *ab*-plane spectra. This indicates that the low energy lattice phonon modes within the herringbone layer are much more sensitive to compression of the crystal lattice than those that are perpendicular. This observation parallels the results obtained in the pressure measurements conducted in the 25–75 meV range. Hence, the affect of pressure on the vibrational behavior of both the intramolecular vibrations and lattice phonon modes is anisotropic relative to the layering motif of the crystal structure.

The MD results partitioned into contributions from molecular motions projected along the unit cell axes are given in Fig. 10. The spectra projected along the *a* and *b*

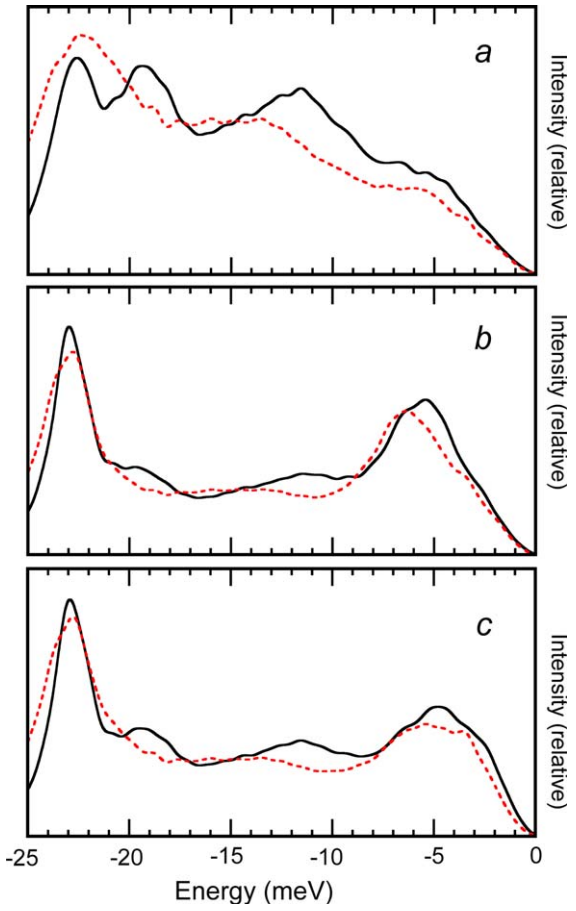

Fig. 10. Comparison of the MD calculated spectra for tetracene at 1 atm (solid line) and 358 MPa (dashed line) projected along the *a*, *b* and *c* unit cell directions between 0 and 25 meV.

Table 7
Assignment of the low energy spectral peaks observed at 295 K and 1 atm relative to the herringbone layer and unit cell axes of tetracene as interpreted from the MD simulation results

Peak	Experimental INS peaks at 295 K, 1 atm	MD assignment relative to herringbone layer	MD assignment relative to unit cell axes
	E (meV)		
1	3.7	z	c
2	5.9	z, ab-plane	a, b, c
3	11.3	ab-plane	a[a]
4	16.6	ab-plane	a[a]
5	20.9	z, ab-plane	a, b, c

[a] Although some contribution from the b and c directions is present in these peaks, the majority of peak intensity is due to vibrational displacements in the a direction.

axes are motions that occur entirely within the herringbone layers. Owing to the triclinic crystal symmetry, however, results in the vibrational spectra in the c direction incorporate motions that are both within and perpendicular to the herringbone layers. Comparing the spectra along the a and b axes permits general features of the ab-plane spectra to be assigned to particular directions within the crystal. Generally, differences in the spectra referenced to the crystal cell as a function of pressure are greatest in the a-direction. In fact, the two experimental peaks displaying the greatest pressure dependent behavior are primarily due to motions occurring in the a-direction. The ab-plane peak at 23 meV incorporates molecular displacements in both the a and b-direction in almost exactly the same proportion. However, the ab-plane peak at $\sim$6 meV has somewhat more motion projected along the b-direction relative to the a-direction. The overall results of this qualitative assignment of the experimental peaks to the unit cell axes has been performed and are given in Table 7 with the assignments relative to the herringbone layer.

4. Conclusions

The crystal structure and vibrational dynamics of tetracene display strongly anisotropic behavior with increasing pressure. The pressure-dependence of the distance and orientation between adjacent molecules is greater within the herringbone layers of the ab crystal plane as opposed to the z-direction perpendicular to the layers. Additionally, changes to both the intramolecular vibrations and lattice phonon parallel the changes observed in the structural anisotropy. Using an ab initio calculation to assign spectral peaks to distinct intramolecular vibrational modes makes clear that intramolecular vibrations with displacements primarily perpendicular to the molecular plane are shifted to higher energy, whereas the intramolecular vibrations that occur within the molecular plane appear constant up to the maximum pressure. The remarkable similarity between the spectra obtained experimentally and by molecular dynamics simulation at both 1 atm and 358 MPa permits the low energy phonons modes to be assigned to particular crystal directions. From these results, the lattice phonon modes are also more strongly affected by increasing pressure if they occur in the layers. Since conduction of tetracene occurs within the herringbone layer, the structural and vibrational features of this study should contribute to a comprehensive understanding of the conduction behavior of tetracene and other similar oligoacene organic semiconductors.

Acknowledgments

The authors thank Dan A. Neumann of the NIST Center for Neutron Research for assistance in the preparation of this manuscript. The authors acknowledge the support of the National Institute of Standards and Technology, U.S. Department of Commerce, in providing the neutron research facilities used in this work. C.D.F. acknowledges partial support by the MRSEC program of the National Science Foundation (DMR #0212302).

References

[1] R.W.I. de Boer, T.M. Klapqijk, A.F. Morpurgo, Appl. Phys. Lett. 83 (2003) 4345.
[2] P.F. Baude, D.A. Ender, M.A. Haase, T.W. Kelley, D.V. Muyres, S.D. Theiss, Appl. Phys. Lett. 82 (2003) 3964.
[3] J.A. Rogers, Z. Bao, K. Baldwin, A. Dodabalapur, B. Crone, V.R. Raju, V. Kuck, H.E. Katz, K. Amundson, J. Ewing, P. Drzaic, Proc. Natl. Acad. Sci. USA 98 (2001) 4835.
[4] F. Garnier, R. Hajlaoui, A. Yassar, P. Srivastava, Science 265 (1994) 1684.
[5] H. Sirringhaus, N. Tessler, R.H. Friend, Science 280 (1998) 1741.
[6] D. Knipp, R.A. Street, A. Volkel, J. Ho, J. Appl. Phys. 93 (2003) 347.
[7] H. Sirringhaus, P.J. Brown, R.H. Friend, M.M. Nielsen, K. Bechgaard, B.M.W. Langeveld-Voss, A.J.H. Spiering, R.A.J. Janssen, E.W. Meijer, P. Herwig, D.M. De Leeuw, Nature 401 (1999) 685.
[8] R.J. Chesterfield, C.R. Newman, T.M. Pappenfus, P.C. Ewbank, M.H. Haukaas, K.R. Mann, L.L. Miller, C.D. Frisbie, Adv. Mater. 15 (2003) 1278.
[9] C. Liu, A.J. Bard, Nature 418 (2002) 162.
[10] Z. Rang, A. Haraldsson, D.M. Kim, P.P. Ruden, M.I. Nathan, R.J. Chesterfield, C.D. Frisbie, Appl. Phys. Lett. 79 (2001) 2731.
[11] M. Chandrasekhar, S. Guha, W. Graupner, Adv. Mater. 13 (2001) 613.
[12] X. Chi, M.E. Itkis, R.W. Reed, R.T. Oakley, A.W. Cordes, R.C. Haddon, J. Phys. Chem. B 106 (2002) 8278.
[13] E.B. Lopes, H. Alves, F. Ribera, M. Mas-Torrent, P. Auban Senzier, E. Canadell, R.T. Henriques, M. Almeida, E. Mohns, J. Veciana, C. Rovira, D. Jérome, Eur. Phys. J. B 29 (2002) 27.
[14] G. Mihály, I. Kézsmárki, F. Zámborszky, L. Forró, Phys. Rev. Lett. 84 (2000) 2670.
[15] H. Tanaka, A. Kobayashi, A. Sato, H. Akutsu, H. Kobayashi, J. Am. Chem. Soc. 121 (1999) 760.
[16] O. Ostroverkhova, D.G. Cooke, S. Shcherbyna, R.F. Egerton, F.A. Hegmann, R.R. Tykwinski, J.E. Anthony, Phys. Rev. B 71 (2005) 035204.
[17] E.A. Silinsh, A. Klimkans, S. Larsson, V. Capek, Chem. Phys. 198 (1995) 311.
[18] E. Silinsh, V. Capek, Organic Molecular Crystals: Interaction, Localization, and Transport Phenomena, American Institute of Physics, New York, 1994.
[19] M. Pope, C.E. Swenberg, Electronic Processes in Organic Crystals and Polymers, second ed., Oxford University Press, New York, 1999.

[20] K.C. Kao, W. Hwang, Electrical Transport in Solids: with Particular Reference to Organic SemiconductorsInternational Series in the Science of the Solid State, vol. 14, Pergamon Press, New York, 1981.
[21] B. Movaghar, J. Mol. Electron. 3 (1987) 183.
[22] Z. Rang, M.I. Nathan, P.P. Ruden, V. Podzorov, M.E. Gershenson, C.R. Newman, C.D. Frisbie, Appl. Phys. Lett. 86 (2005) 123501/1.
[23] R.G. Kepler, in: J.J. Brophy, J.W. Buttrey (Eds.), Organic Semiconductors, Macmillan, London, 1962, p. 1.
[24] J. Kalinowski, J. Godlewski, R. Jankowiak, Chem. Phys. Lett. 43 (1976) 127.
[25] R. Jankowiak, H. Bässler, A. Kutoglu, J. Phys. Chem. 89 (1985) 5705.
[26] E. Venuti, R.G. Della Valle, L. Farina, A. Brillante, Phys. Rev. B 70 (2004) 104106.
[27] Details of the Harwood Engineering two-piston pressure intensifier system available for use at the NCNR can be found at: <http://users.rcn.com/harwood.ma.ultranet/prim200k.html>.
[28] The BT-1 high resolution neutron powder diffractometer instrument is described at the NCNR website address: <http://www.ncnr.nist.gov/instruments/bt1/>.
[29] A.C. Larson, R.B. Von Dreele, General Structure Analysis System (GSAS), Los Alamos National Laboratory Report LAUR 86-748, 2000.
[30] B.H. Toby, J. Appl. Crystallogr. 34 (2001) 210.
[31] R.B. Campbell, J.M. Robertson, J. Trotter, Acta Crystallogr. 15 (1962) 289.
[32] One is directed to the NCNR website at: <http://www.ncnr.nist.gov/instruments/fans/> for more detailed information on the BT-4 FANS instrument.
[33] One is directed to the NCNR website at: <http://www.ncnr.nist.gov/instruments/fcs/> for more detailed information on the BT-4 FANS instrument.
[34] S.R. Langhoff, J. Phys. Chem. 100 (1996) 2819.
[35] T. Kato, T. Yamabe, J. Chem. Phys. 115 (2001) 8592.
[36] M. Malagoli, V. Coropceanu, D.A. da SilvaFilho, J.L. Bredas, J. Chem. Phys. 120 (2004) 7490.
[37] Detailed information regarding Gaussian 98 can be found at: <http://www.Gaussian.com>.
[38] A.M. Pivovar, M.D. Ward, C.M. Brown, D.A. Neumann, J. Phys. Chem. B 106 (2002) 4916.
[39] A.D. Mackerell Jr., D. Bashford, M. Bellott, R.L. Dunbrack Jr., J.D. Evanseck, M.J. Field, S. Fischer, J. Gao, H. Guo, S. Ha, D. Joseph-McCarthy, L. Kuchnir, K. Kuczera, F.T.K. Lau, C. Mattos, S. Michnick, T. Ngo, D.T. Nguyen, B. Prodhom, W.E. Reiher III, B. Roux, M. Schlenkrich, J.C. Smith, R. Stote, J. Straub, M. Watanabe, J. Wiorkiewicz-Kuuczera, D. Yin, M. Karplus, J. Phys. Chem. B 102 (1998) 3586.
[40] Gaussian 03, Revision A.1, Gaussian Inc., Pittsburgh, PA.
[41] C.I. Bayly, P. Cieplak, W.D. Cornell, P.A. Kollman, J. Phys. Chem. 97 (1993) 10269.
[42] U. Essmann, L. Perera, M.L. Berkowitz, T. Darden, L.G. Pedersen, J. Chem. Phys. 103 (1995) 8577.
[43] G.J. Martyna, M.E. Tuckerman, M.L. Klein, J. Chem. Phys. 97 (1992) 2635.
[44] G.J. Martyna, D.J. Tobias, M.L. Klein, J. Chem. Phys. 101 (1994) 4177.
[45] G.J. Martyna, M.E. Tuckerman, D.J. Tobias, M.L. Klein, Mol. Phys. 87 (1996) 1117.
[46] M.E. Tuckerman, D.A. Yarne, S.O. Samuleson, A.L. Hughes, G.J. Martyna, Comput. Phys. Comm. 128 (2000) 333.
[47] M.P. Allen, D.J. Tildesley, Computer Simulation of Liquids, Clarendon Press, Oxford, 1987.
[48] M. Oehzelt, R. Resel, A. Nakayama, Phys. Rev. B 66 (2002) 174104.
[49] U. Sonderman, A. Kotuglu, H. Bässler, J. Phys. Chem. 89 (1985) 1735.
[50] M. Oehzelt, G. Heimel, R. Resel, P. Pushnig, K. Hummer, C. Ambrosch-Draxl, K. Takemura, A. Nakayama, J. Chem. Phys. 119 (2003) 1078.
[51] P. Puschnig, K. Hummer, C. Ambrosch-Draxl, G. Heimel, M. Oehzelt, R. Resel, Phys. Rev. B 67 (2003) 235321.
[52] G. Heimel, P. Puschnig, M. Oehzelt, K. Hummer, B. Koppelhuber-Bitschnau, F. Porsch, C. Ambrosch-Draxl, R. Resel, J. Phys. Condens. Matter 15 (2003) 3375.
[53] G. Filippini, C.M. Gramaccioli, Chem. Phys. Lett. 104 (1984) 50.
[54] B. Dorner, E.L. Bokhenkov, S.L. Chaplot, J. Kalus, I. Natkaniek, G.S. Pawley, U. Schmelzer, E.F. Sheka, J. Phys. C: Solid State Phys. 15 (1982) 2353.
[55] R.G. Della Valle, E. Venuti, L. Farina, A. Brillante, M. Masino, A. Girlando, J. Phys. Chem. B 108 (2004) 1822.